Journal of Hazardous Materials 366 (2019) 39–45

Contents lists available at ScienceDirect

Journal of Hazardous Materials

journal homepage: www.elsevier.com/locate/jhazmat

Electrocoagulation using aluminium anodes activated with Mg, In and Zn alloying elements

Adelaide Dura, Carmel B. Breslin*

Department of Chemistry, Maynooth University, Maynooth, County Kildare, Ireland

ARTICLE INFO

Keywords:
Aluminium alloy
Al–Zn–In
Al–Mg
Electrocoagulation
Phosphate
Orange II
Zinc ions

ABSTRACT

The simultaneous removal of phosphates, Zn^{2+} and Orange II, in two synthetic wastewaters was achieved using Al–Mg and Al–Zn–In alloys as anodes at 11.7 mA cm^{-2} and a surface area to volume ratio of 19.0 m^{-1}. Higher removal efficiencies were obtained with Al–Zn–In, attaining values of 95–96% for phosphate, 99% for Zn^{2+} and 88–96% for Orange II, while somewhat lower values were seen with Al–Mg, with 89–93% for phosphate, 96% for Zn^{2+} and 50–60% for Orange II, depending on the solution. The higher efficiency with Al–Zn–In was attributed to its less passive behaviour, which was evident from polarisation plots. Numerous shallow pits, resembling general–like dissolution, were seen with Al–Zn–In, while fewer and larger pits were observed with Al–Mg. The energy demand for the removal of the pollutants was computed as 1.30 and 2.55 kWh m^{-3} for the Al–Zn–In and Al–Mg anodes, respectively. The removal of phosphates and Orange II was explained in terms of the generation of cationic polynuclear aluminium species that provide electrostatic interactions with the anionic phosphates and Orange II. The removal of Zn^{2+} was attributed to the formation of insoluble $Zn(OH)_2$.

1. Introduction

Electrocoagulation consists of delivering metallic hydroxide flocs to wastewater by the electrodissolution of electrodes which act as sacrificial anodes [1–3]. Electrocoagulation dates back to the early 1900s when aluminium and iron electrodes were first employed [1]. However, as a result of the expensive electricity supply coupled with the availability of mass–produced alternatives for chemical coagulant dosing, electrochemical treatment of water did not find widespread applications [2]. In recent times, there has been a renewed interest in electrocoagulation [1–7]. The electrocoagulation process is particularly suited to small treatment technologies, while larger centralised treatment facilities are still a challenge [5]. Electrocoagulation has a number of advantages over other water treatment technologies [8]. The occurrence of secondary pollution is minimised as no chemicals are added. It produces low amounts of sludge and the flocs can be easily separated by filtration. The gas bubbles produced during electrolysis at the cathode can carry the light flocs to the top of the reactor where they can be easily collected and removed. Finally, the energy required for the process can be provided by green energy, such as wind power or solar panels [6]. Electrocoagulation has been shown to remove a wide range of pollutants, including heavy metals [3,7], textiles, organic pollutants and petroleum products [3]. This ability to remove a wide range of contaminants accounts for the increasing interest in the electrocoagulation process.

Electrocoagulation has been extensively investigated and a number of mechanistic studies has been reported [9,10]. Electrodissolution, coagulation and flotation are all identified as key elements [5]. Considerable attention has been devoted to identifying the key underlying mechanisms of pollutant removal, however few researchers have addressed the nature of the electrode material employed, and most of these studies focus on comparing aluminium and iron anodes [11]. The performance and energy efficiency, while depending on the configuration of the electrocoagulation cell and the connection of the anodes, are also related to the reactions occurring at the electrode–solution interface. In particular, the formation of passive films or oxides, inhibits dissolution and restricts the charge–transfer reaction at the anode–solution interface and this leads to excessive consumption of electricity and reduces the energy efficiency of the process [12]. In the presence of chloride anions, passive anodes become susceptible to pitting and localised corrosion and this leads to the non–uniform dissolution of the anode. Furthermore, with higher concentrations of chloride, the overconsumption of the anode occurs due to more severe pitting attack [13].

Pure aluminium forms a passive layer in aqueous solutions and in the presence of chloride anions pits nucleate and propagate to give deep

* Corresponding author.
E-mail address: Carmel.Breslin@mu.ie (C.B. Breslin).

https://doi.org/10.1016/j.jhazmat.2018.11.094
Received 7 October 2018; Received in revised form 21 November 2018; Accepted 23 November 2018
Available online 24 November 2018
0304-3894/

pits distributed across the surface [14]. Repassivation of these pits can occur, however, it is even more difficult to induce metal dissolution at these sites. The composition of the electrocoagulation solution plays a role in the extent of pitting attack, with chloride anions giving rise to the initiation of pits, while sulfates and phosphates act as inhibitors [15,16]. It is no surprise that pure aluminium gives problems when used as the anode [17], as its dissolution is through pitting attack. In contrast, general-like dissolution is more attractive, giving a near uniform rate of dissolution that can be controlled to deliver the required concentration of metal cations.

In this study, two aluminium alloys, Al–Mg and Al–Zn–In, were selected and used as anodes in an electrocoagulation study. These alloys were selected as zinc and indium alloying components, in particular, are well known to activate aluminium [18,19]. This activation process results in the destabilisation of the passive film making these alloys interesting candidates for electrocoagulation. The corrosion and passive behaviour of Al–Mg and Al–Zn–In was initially studied and compared with pure Al and then the alloys were used to remove phosphates, Zn^{2+} cations and Orange II. These three pollutants were chosen as they are removed by different processes. To the best of our knowledge, these alloys have not been previously used in the removal of phosphates, heavy metal cations or dye molecules. Instead, aluminium anodes, typically at 99.9% to 99.5% purity have been employed [2,5,17].

2. Experimental method

All chemicals were supplied by Sigma–Aldrich®. All electrolyte solutions were prepared using deionised water. The electrocoagulation tests were carried out in two synthetic wastewaters, sww1 and sww2, which were formulated from the OECD synthetic sewage [20] and contained some of the ions most commonly present in wastewater. The composition of the two solutions is shown in Table 1 and they vary in terms of the chloride content, which is present as NaCl and $CaCl_2$, to give a 7–fold increase in the chloride concentration and a 4–fold increase in the conductivity as sww1 is replaced by sww2.

All metals and alloys were supplied by Goodfellow© in rod and sheet forms. The rod electrodes were used in corrosion studies, while the sheets were used in electrocoagulation tests. The Al-Mg (1.7–2.4% Mg, 0.5% Fe, 0.5–0.1% Mn, 0.4% Si, balance Al), Al–Zn–In (3% Zn, 0.02% In, 0.12% Fe, 0.08% Si, 0.006% Cu, balance Al) and high purity Al (99.99%) rod electrodes were set in a Teflon® holder with epoxy resin. Electrical contact was made using a copper wire, which was threaded to the base of the sample. The exposed electrode surface was abraded on a Buehler® Metaserve grinder polisher with water lubricated Buehler® SiC grinding papers to a 2500 grit finish. The electrodes were then polished with successively finer grades of Buehler® MetaDi monocrystalline diamond suspensions ranging from 30 to 1 µm on Buehler® polishing microcloths and sonicated and dried in a stream of air. The samples used in the electrocoagulation tests were cut to form sheets. For comparison, pure Al (99.9%) anodes were also employed. Before each experiment the sheets were abraded with water lubricated Buehler® silicon carbide paper (Grit P 320 to P 2500), washed with deionised water and dried in a stream of air.

The polarisation and cyclic polarisation experiments were carried out in a three–electrode cell with a saturated calomel electrode and a high surface area platinum wire as the counter electrode. The electrodes were immersed in the solution for a 30–min period and then polarised in the anodic direction from about 300 mV below the corrosion potential, E_{corr}, at 0.5 mV s^{-1}. For the cyclic polarisation experiments, the scan was reversed at a current density of 1 mA cm^{-2} and the electrode was polarised in the reverse direction. The electrocoagulation tests were carried out at room temperature using a two–electrode cell with a steel cathode (AISI 310) and Al–Mg or Al–Zn–In as the anode. The distance between the anode and the cathode was maintained at 1 cm. A constant current density of 11.7 mA cm^{-2} was applied and the solution was agitated. The ratio of the surface area of the anode to the volume of solution (SA/V) was fixed at 19.0 m^{-1}. Samples were periodically taken and allowed to settle for 15 min. Then the supernatant was filtered with Whatman™ filter paper and analysed for the required quantitative determination. The efficiency of removal, η, was computed according to Eq. (1), where C_0 is the initial concentration and C_t is the concentration of the analyte at time *t*.

$$\eta(\%) = \frac{C_0 - C_t}{C_0} \times 100 \quad (1)$$

UV–Vis spectroscopy was used to determine the concentrations of phosphate and Orange II. A Unicam Thermo Spectronic® UV 540 double–beam spectrometer was used. The phosphate concentration was measured according to the vanadomolybdophosphoric acid colorimetric method [21] to give an absorption maximum at 470 nm, while the Orange II concentration was obtained by monitoring the absorption peak at 485 nm. In order to avoid interference, the spectrophotometric determination of phosphate and Orange II was carried out by solving the simultaneous linear equations given in Eq. (2). In this analysis, A_{470} and A_{485} are the absorbance values from the spectrum of the mixture at 470 nm and 485 nm, ε^p_{470} and ε^p_{485} are the molar absorptivities of phosphate at 470 and 485 nm computed from the spectrum of pure phosphate. Likewise, ε^o_{470} and ε^o_{470} are the molar absorptivities of Orange II at 470 nm and 485 nm computed from the spectrum of the Orange II, and C_P and C_o are the concentrations of phosphate and Orange II, respectively. Therefore, the concentrations of the two components were obtained by recording the absorbance at 470 nm and 485 nm and solving Eq. (2).

$$\begin{aligned} A_{470} &= \varepsilon^p_{470} C_P + \varepsilon^o_{470} C_o \\ A_{485} &= \varepsilon^p_{485} C_P + \varepsilon^o_{485} C_o \end{aligned} \quad (2)$$

The concentrations of Zn^{2+} in the coagulant were obtained using AA spectroscopy with a Perkin Elmer Analyst 200 atomic absorption spectrometer at 213.9 nm. The standard solutions were prepared by dissolving metallic zinc in HNO_3. Optical micrographs were recorded using an Olympus® BX51 M microscope in a dark–field mode. The micrographs were taken with a computer interfaced to a CCD camera (Leica DFC 2280 digital camera) and Olympus® DP version 3.2 software.

3. Results

3.1. Passive and dissolution behaviour of Al, Al–Mg and Al–Zn–In

Typical polarisation curves are shown in Fig. 1 for pure Al recorded in aqueous solutions with chloride concentrations between 5 mM and 0.5 M NaCl. The passive behaviour of Al is clearly evident with a near constant passive current of 5×10^{-5} A cm^{-2} to 8×10^{-5} A cm^{-2}. There is a significant variation in the breakdown potential, which ranges from

Table 1
Composition of the electrolyte solutions, sww1 and sww2, used in the electrocoagulation tests. The pH was maintained at 5.0.

	$CaCl_2.2H_2O$ g L^{-1}	$MgSO_4.7H_2O$ g L^{-1}	NaCl g L^{-1}	PO_4-P mg L^{-1}	Orange II mg L^{-1}	Zn^{2+} mg L^{-1}	κ mS m^{-1}
sww 1	0.4	0.2	0.7	500	50	100	3.7
sww 2	0.4	0.2	7.0	500	50	100	14.4

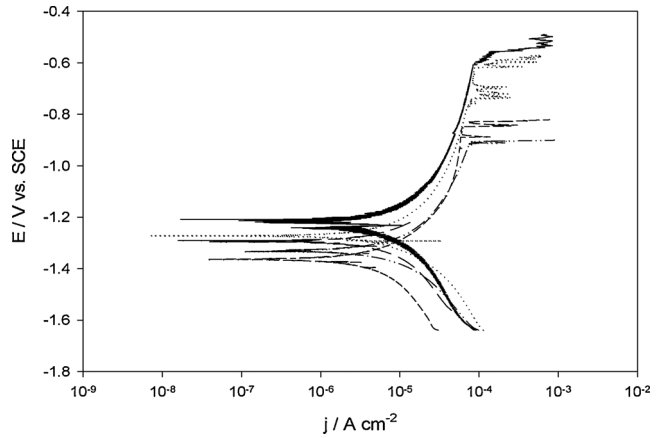

Fig. 1. Polarisation curves recorded at 0.5 mV s^{-1} for pure aluminium in —— 5 mM, · · · 0.01 M, – – – 0.10 M, – ·· – 0.25 M and — — — 0.50 M NaCl.

–0.55 V vs. SCE in 5 mM NaCl to approximately –0.90 V vs. SCE in 0.5 M NaCl. Current fluctuations are observed below the breakdown potential and these transients can be attributed to the occurrence of metastable pits which form and repassivate at potentials below the breakdown potential. On the addition of phosphates (data not shown) to the solution, the breakdown potential was displaced to higher potentials. Similar effects were seen with sulfates. Sulfates and phosphates are well–known corrosion inhibitors [15,16]. As phosphates and sulfates are often found in solutions with relatively low chloride concentrations, these data highlight the limitations of using pure Al, which is not only prone to pitting attack, but develops a more protective passive oxide layer in the presence of phosphates and sulfates.

In Fig. 2(a) cyclic polarisation curves are shown for Al–Mg recorded in sww1 and sww2. These plots were obtained by cycling the electrodes from –0.90 V vs. SCE and the cycle was reversed when a current density of 1.0 mA cm^{-2} was achieved. The extended passive region seen in Fig. 1 is no longer evident. The breakdown and corrosion potentials are similar and the current fluctuations, seen in Fig. 1, are now largely removed. Once the potential exceeds the corrosion potential, E_{corr}, dissolution of the alloy occurs. It is apparent that the cyclic polarisation curves exhibit hysteresis. The size of the hysteresis loop is smaller in sww1. These two solutions differ in terms of the chloride content with a 7–fold increase in the chloride concentration for sww2. This indicates somewhat more dissolution with the higher chloride concentration, which is in good agreement with several studies [22], where it is normally accepted that higher chloride concentrations give rise to higher degrees of pit acidification and more dissolution. The distribution and morphology of pits formed at Al–Mg in the sww1 and sww2 solutions are shown in Fig. 2(b) and (c), respectively. Pits with different diameters ranging from 20 to 80 µm are visible.

The influence of sulfates is evident in Fig. 3(a) which compares the polarisation curves recorded in 0.017 M NaCl and in 0.017 M NaCl with added sulfate (0.81 mM). In the presence of sulfate, E_{corr} occurs at –0.50 V vs. SCE, about 60 mV higher than that obtained in the absence of sulfates. In Fig. 3(b) and (c) the corresponding micrographs are presented. In the absence of any corrosion inhibitors, Fig. 3(b), clusters of several small pits are seen. The diameters of the clusters were calculated as 110 ± 10 µm. These clusters become less developed in the presence of sulfates, Fig. 3(c), phosphates or in the sww1 and sww2 solutions, Fig. 2 (b) and (c). These observations are in good agreement with the existing literature on the effects of sulfate ions on the pitting corrosion of aluminium [15,16] where sulfates are shown to retard pit initiation and growth.

The polarisation behavior of Al–Zn–In is shown in Fig. 4 (a), while the corresponding micrographs are presented in Fig. 4(b) and (c), respectively. Above E_{corr} active dissolution is observed and again there is no evidence of any passive region. In sww2, which contains the higher concentration of chloride, the increase in current above the corrosion potential is more rapid, giving a higher gradient. The corresponding micrographs recorded after the cyclic scans in sww1 and sww2, reveal the existence of pitting corrosion. However, the density of pits is high, and the pits are relatively small and shallow in both the sww1 and sww2 solutions. Again, there was evidence of corrosion inhibition afforded by the presence of sulfates and phosphates in sww1 and sww2. There was an increase in the corrosion potential, E_{corr}, from approximately –1.08 V vs. SCE in 0.12 M NaCl to –0.86 V vs. SCE in sww1, while in the presence of 0.017 M NaCl, E_{corr} was about –0.91 V vs. SCE and increased to –0.79 V vs. SCE in sww1 (data not shown for the chloride solutions).

The dependence of these dissolution reactions on the chloride concentration is summarised in Fig. 5, where a linear relationship is obtained between the breakdown potential, E_{br}, and the logarithm of the chloride concentration, Eq. (3). The constant B was computed as –0.20 V for pure Al, –0.12 V for Al–Zn–In and –0.10 V for Al–Mg, indicating a high dependence between the chloride concentration and the breakdown potential for pure Al. This high dependence on chloride concentration and the extended passive region will have a negative effect on the performance of pure Al in electrocoagulation. The chloride concentration has less influence on the breakdown potentials of Al–Mg and Al–Zn–In.

$$E_{br} = A - B \log [Cl^-] \quad (3)$$

On comparing the data obtained with the two alloys, it is evident

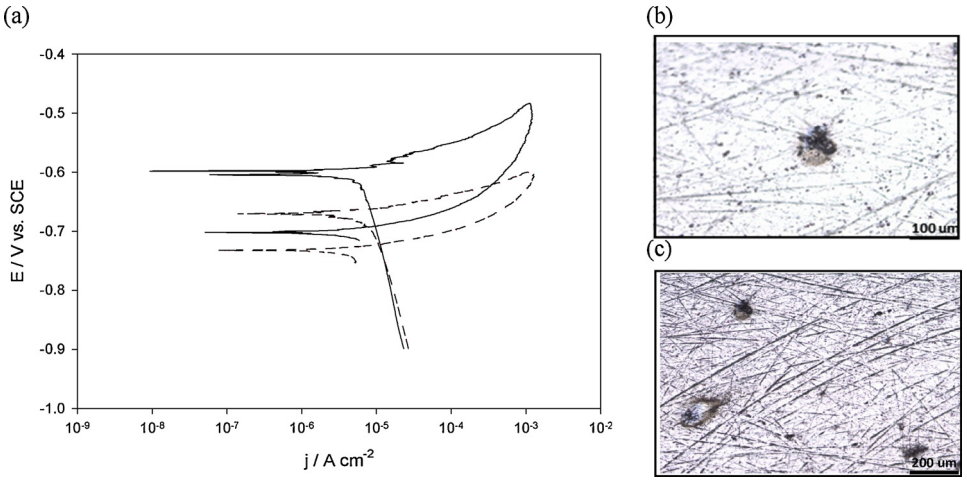

Fig. 2. (a) Cyclic polarisation curves recorded at 0.5 mV s^{-1} for Al–Mg in —— sww1 and – – – sww2, micrographs of Al–Mg in (b) sww1 and (c) sww2.

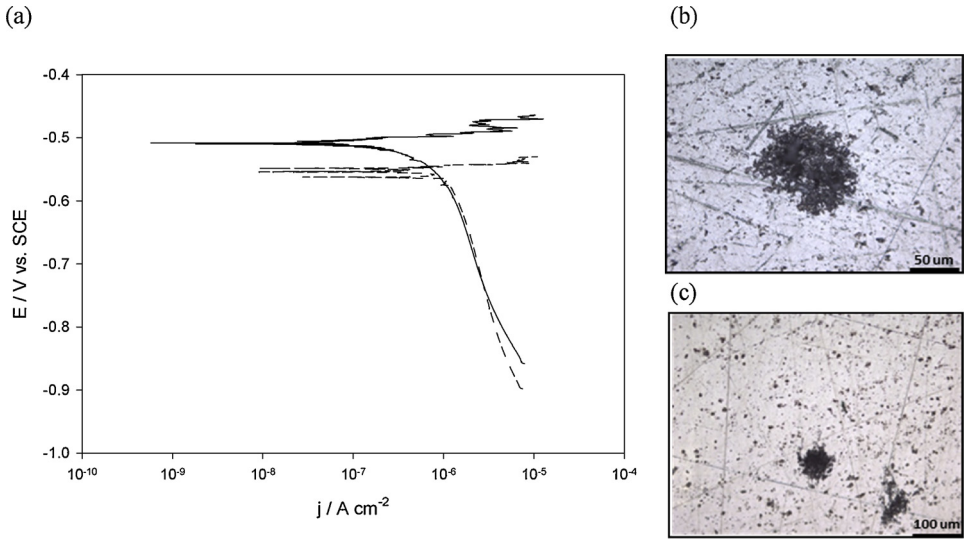

Fig. 3. (a) Polarisation curves recorded at 0.5 mV s^{-1} for Al–Mg in —— 0.017 M NaCl and 8.1 × 10^{-4} M Na_2SO_4, pH 5.0 and – – – 0.017 M NaCl, pH 5.0, micrographs recorded for Al–Mg in (b) 0.017 M NaCl and in (c) 0.17 M with added sulfate.

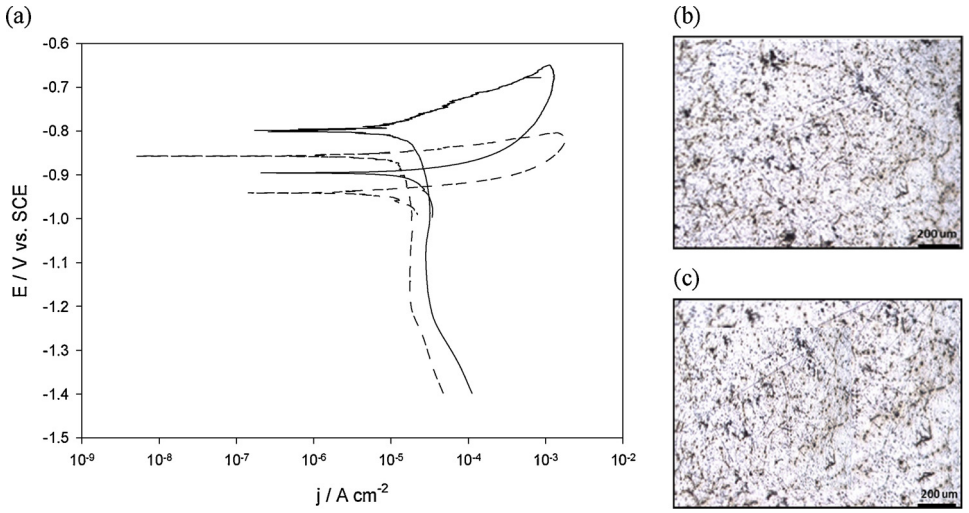

Fig. 4. (a) Cyclic polarisation curves recorded at 0.5 mV s^{-1} for Al–Zn–In in —— sww1 and – – – sww2; micrographs of Al–Zn–In in (b) sww1 and (c) sww2.

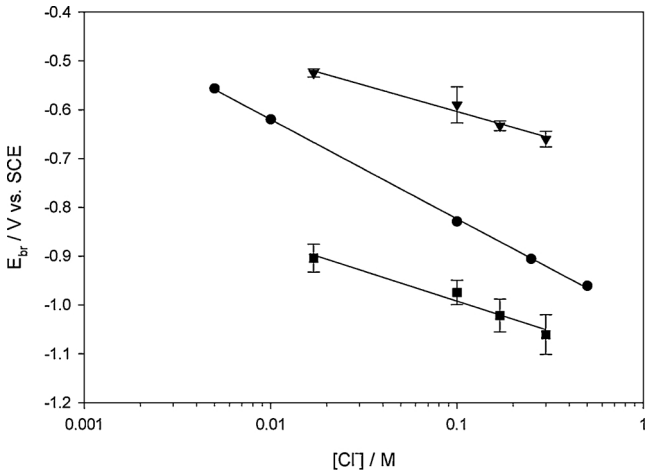

Fig. 5. Breakdown potentials, E_{br}, of ▼ Al–Mg, ● pure aluminium, and ■ Al–Zn–In electrodes plotted as a function of the logarithm of the chloride concentration.

that a large number of smaller pits nucleate at Al–Zn–In, while fewer pit nucleation sites are evident with the Al–Mg alloy. In Fig. 2 and 4, the potential was reversed at 1 mA cm^{-2} to give similar overall dissolution currents, which suggests that more general–like dissolution occurs with Al–Zn–In while fewer pits develop to give the required current with Al–Mg. This may be related to the more passive behavior of Al–Mg, making it more difficult to nucleate the pits. Once they are nucleated they are capable of giving the required current and delivering high concentrations of Al^{3+}. This in turn gives rise to more developed and deeper pits. However, the most significant difference between both alloys is the applied potential at which pitting and dissolution become apparent, with the Al–Zn–In undergoing dissolution at more negative potentials, with E_{corr} at –0.67 V vs. SCE for Al–Mg and at –0.86 V vs. SCE for Al–Zn–In in sww2.

3.2. Electrocoagulation – removal of phosphates, Zn^{2+} and orange II

The removal of phosphates from sww1 and sww2 is shown in Fig. 6, where the residual concentrations of PO_4–P are plotted as a function of time for the Al–Mg and Al–Zn–In electrodes. Pseudo first–order plots are shown in the inset, where the logarithm of the phosphate concentration is plotted as a function of time. The computed efficiencies

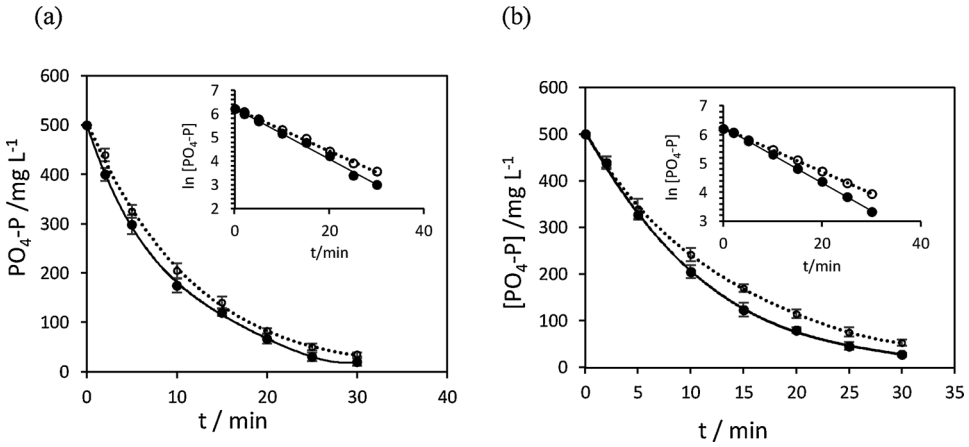

Fig. 6. Residual concentration of PO_4–P for —●— Al–Zn–In and ··· ○··· Al–Mg plotted as a function of the electrocoagulation time in (a) sww1 and (b) sww2.

Table 2
Efficiency over a 30–min period and pseudo first–order rate constant for the removal of phosphate.

System	Solution	η / %	k_{obs} / min^{-1}
Al–Zn–In	sww1	95	0.092
	sww2	96	0.108
Al–Mg	sww1	89	0.075
	sww2	93	0.091

Table 3
Efficiency over a 20–min period and pseudo first–order rate constant for the removal of Zn^{2+}.

System	Solution	η / %	k_{obs} / min^{-1}
Al–Zn–In	sww1	99.2	0.241
	sww2	99.8	0.311
Al–Mg	sww1	96.0	0.161
	sww2	96.0	0.164

and pseudo first–order rate constants, k_{obs}, are summarised in Table 2. It is clear that the Al–Zn–In anodes exhibit a slightly better removal, however both anodes perform well in removing the phosphate with removal efficiencies greater than 90%. As shown in Table 1, there is a 4–fold increase in the conductivity of the test solution and a 7–fold increase in the total chloride concentration on comparing sww1 and sww2. This appears to have little influence on the removal efficiencies, with only a slight increase for the Al–Zn–In system over a 30–min period from 93% to 96%. Using a 99.9% pure Al anode (data not shown), lower efficiencies were obtained, with an efficiency of 65% in sww1 and 76% in sww2. As shown in Figs. 1 to 4, dissolution of the alloys is evident at low overpotentials to give relatively high concentrations of Al^{3+}, while pure Al is more passive.

The removal performances of Al–Mg and Al–Zn–In in removing Zn^{2+} ions are summarised in Fig. 7 and Table 3. Very good removal of the Zn^{2+} ions is achieved with both alloys within 15 min. Furthermore, the conductivity and the chloride concentration of the solutions have little effect on the efficiencies which range from 96 to 99%, Table 3. Nevertheless, the rate constants are slightly higher for the Al–Zn–In alloy. These results are consistent with the precipitation of zinc hydroxide, $Zn(OH)_2$. During the electrocoagulation experiment, the pH varied from an initial pH of 5.0 to a final pH of 8.9 ± 0.5 for the bulk solution, in agreement with previous reports [13]. The speciation diagram for an aqueous zinc solution [23] is displayed in Fig. 8 and shows that the predominant species in the pH range of 8.5 to 10.5 is $Zn(OH)_2$. The bulk solution with a final pH value of approximately 8.9, is sufficiently alkaline to generate $Zn(OH)_2$, facilitating the removal of Zn^{2+} through the formation of insoluble $Zn(OH)_2$.

In Fig. 9 the residual concentrations of Orange II are plotted as a function of the electrocoagulation period for the Al–Mg and Al–Zn–In electrodes. It is clearly evident that the removal of the dye molecule is much slower compared to the phosphate anions. However, after about 40 min the removal efficiency of Al–Zn–In reaches 96%. The Al–Mg alloy exhibits a much lower removal of the dye, with an efficiency of

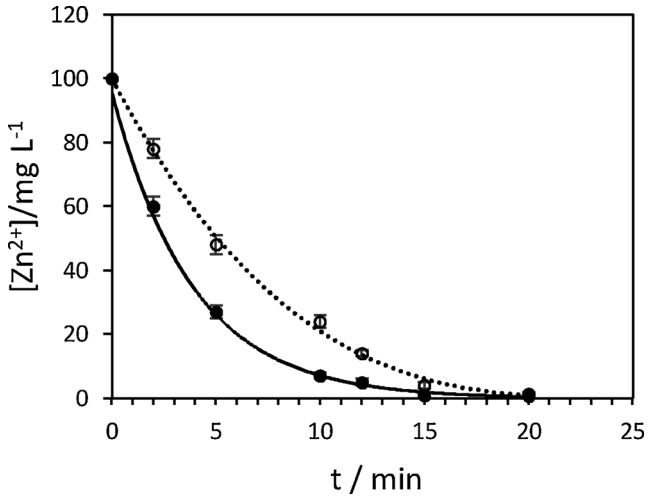

Fig. 7. Residual concentration of Zn^{2+} for —●— Al–Zn–In and ··· ○··· Al–Mg plotted as a function of the electrocoagulation time in sww1.

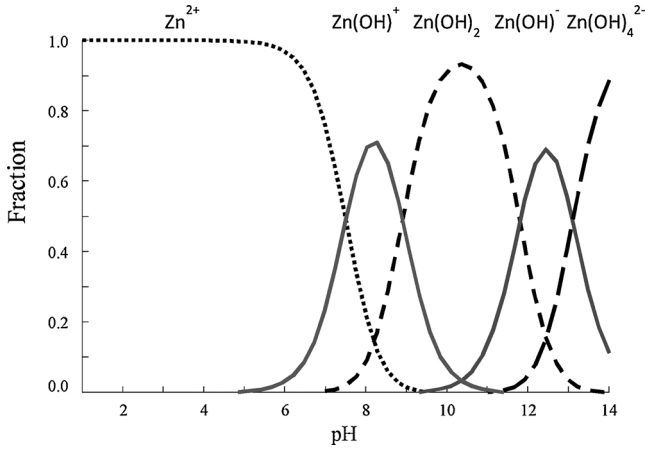

Fig. 8. Speciation diagram of zinc in solutions, calculated using the SOLGASWATER algorithm [23].

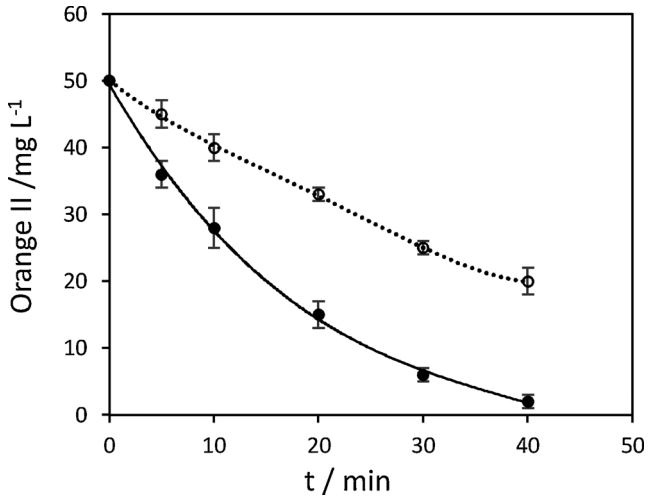

Fig. 9. Residual concentration of Orange II for —●— Al–Zn–In and ··· ○··· Al–Mg plotted as a function of the electrocoagulation time in sww2, with i = 11.7 mA cm^{-2}.

Table 4
Efficiency over a 40–min period and pseudo first–order rate constant for the removal of Orange II.

System	Solution	η / %	k_{obs} / min^{-1}
Al–Zn–In	sww1	88	0.055
	sww2	96	0.078
Al–Mg	sww1	50	0.017
	sww2	60	0.023

only 50% in sww1 and about 60% in sww2 following a 40–min electrocoagulation period (Table 4). The performance of the pure Al anode (data not shown) in removing Orange II was particularly poor, with an efficiency of only 23% in both sww1 and sww2.

Another important parameter is the energy consumption during electrocoagulation. The energy supplied to the system is expressed in terms of specific electrical energy consumption, SEEC, Eq. (4), where E_{cell} is the cell voltage, I is the current, t is the time and V is the volume of solution treated [3]. The data obtained using Eq. (4) are summarised in Table 5.

$$SEEC = \frac{E_{cell} \times I \times t}{V} \quad (4)$$

It is apparent that the Al–Zn–In electrode is consistently more efficient in terms of energy in both test solutions. Higher energy consumption is exhibited by the Al–Mg electrode, with 5.15 Wh m^{-3} in sww1 and 2.55 Wh m^{-3} in the sww2 solution. The energy demand diminishes considerably in the sww2 solution. This is not surprising as the solution conductivity, κ, affects the cell voltage, E_{cell}, by reducing the ohmic drop. The corrosion potentials obtained from the polarisation data are also provided in Table 5 and in general, low values of E_{corr} result in greater energy efficiency.

Table 5
Energy consumption, SEEC, i = 11.7 mA cm^{-2}, t = 30 min and SA/V = 19.1 m^{-1} and E_{corr} was obtained from polarisation data.

System	Solution	SEEC /kWh m^{-3}	E_{corr} / V vs. SCE
Al–Zn–In	sww1	1.95	–0.79
	sww2	1.30	–0.86
Al–Mg	sww1	5.15	–0.58
	sww2	2.55	–0.67

4. Discussion

It is clear from Figs. 6, 7 and 9 that the Al–Zn–In alloy, and the Al–Mg alloy to a lesser extent, perform well in the simultaneous removal of phosphates, Zn^{2+} ions and Orange II. The removal of phosphates compares well to previous reports. For example, Irdemez et al. [24] reported a removal efficiency of 88% for an initial phosphate concentration of 150 mg L^{-1}, while Bektas et al. [25] obtained a removal efficiency of 90% for an initial concentration of 200 mg L^{-1}. The initial concentration used in this study is higher at 500 mg L^{-1}. It is known that higher removal efficiencies are achieved with lower initial phosphate concentrations [26]. This illustrates good efficiencies for both Al–Zn–In at 96% and the Al–Mg anode at 93%, in 500 mg L^{-1} phosphate in the presence of several other ions.

The removal of Zn^{2+} is particularly efficient and this is largely connected with the generation of an alkaline solution and the formation of insoluble $Zn(OH)_2$ [27,28]. However, the reduction of Zn^{2+} to metallic Zn at the cathode is a possible reaction, Eq. (5). The reduction potential for this reaction using the initial concentration of Zn^{2+} (1.52 mM) and the Nernst equation is –0.81 V vs. SHE, while the standard reduction potential for the reduction of H^+, Eq. (6), at a pH of 5.0 is given by Eq. (7), and the reduction potential for the electrolysis of water, Eq. (8), is –0.83 V vs. SHE. Initially at a pH of 5.0, Eq. (6) will occur. However, as the interfacial pH at the cathode increases, Eq. (8) will predominate and now the standard reduction potentials for Eqs. (5) and (8) are similar, giving rise to the possible reduction of Zn^{2+}.

$$Zn^{2+} + 2e^- \rightarrow Zn \quad (5)$$

$$2H^+ + 2e^- \rightarrow H_2 \quad (6)$$

$$E = E^o - 0.0591\ pH = -0.30\ V \quad (7)$$

$$2H_2O + 2e^- \rightarrow H_2 + 2OH^- \quad (8)$$

The high removal efficiencies of Zn^{2+} ions observed for Al–Mg and Al–Zn–In is accomplished primarily through precipitation in agreement with other reports [28,29]. However, higher initial concentrations of Zn^{2+} may favour the electrodeposition of zinc at the cathode.

It is more difficult to account for the difference between Al–Mg and Al–Zn–In in removing Orange II. While the electrochemical behavior of the electrodes is similar, Figs. 2–4, Al–Zn–In adopts lower breakdown potentials of –0.78 V vs. SCE in sww1 and –0.84 V vs. SCE in sww2, compared to the slightly higher values of –0.58 V and –0.66 V vs. SCE obtained for Al–Mg. The corrosion current density, i_{corr} was calculated using the Tafel equation, Eq. (9). In this expression, $E - E_{corr}$ represents the overpotential, η, where E_{corr} is the corrosion potential, i is the measured current density and i_{corr} represents the corrosion current density. On fitting the polarisation data to the equation, i_{corr} values of 15 μA cm^{-2} in sww1 and 12 μA cm^{-2} in sww2 were obtained for Al–Zn–In, while lower values of 6.5 μA cm^{-2} and 4.6 μA cm^{-2} were computed for Al–Mg in the sww2 and sww1 solutions, respectively. This indicates that Al–Mg is more resistant to dissolution and consequently higher potentials are required to maintain the current at 11.7 mA cm^{-2}. The average cell potential of Al–Zn–In reached 1.37 V and 0.92 V in the sww1 and sww2 solutions, respectively, while higher values of approximately 3.64 V and 1.85 V were recorded for Al–Mg in the sww1 and sww2 solutions, respectively. The higher potentials may give secondary reactions, such as the evolution of oxygen, Eq. (10). This parasitic reaction, which consumes charge, gives rise to lower concentrations of Al^{3+} and aluminium hydrolysis species. It appears from this analysis that the dye interacts with the species generated on the hydrolysis of Al^{3+}. It is well known that the hydrolysis of Al^{3+} proceeds rapidly to give various monomeric, dimeric, trimer and poly–nuclear species [3]. These cationic species will attract the negatively charged sulfonate group (SO_3^-) of the dye molecule. Indeed, given the size of the polymeric aluminium cations and the dye molecule the formation of an ion pair is possible.

$$\eta = E - E_{corr} = \frac{2.303RT}{\alpha F} logi_{corr} - \frac{2.303RT}{\alpha F} logi \quad (9)$$

$$2H_2O \rightarrow O_2 + 4H^+ + 4e^- \quad (10)$$

There may be some competition between the removal of phosphate, Orange II and Zn^{2+}. The formation of $Zn(OH)_2$ due to the removal of Zn^{2+} will probably have little influence on the removal of the dye, however there may be competition between the removal of phosphates and the dye molecules. If the removal of the dye and phosphates is governed by electrostatic interactions with the aluminium hydroxyl species, then the higher initial concentrations of phosphate, will favour its removal. This may explain why there is no significant difference between the two alloys in the removal of phosphates. A sufficient amount of Al^{3+} is formed to remove the phosphates, but the more passive behavior of Al–Mg becomes evident in the removal of the dye.

The better performance of the Al–Zn–In alloy appears to be related to its ease of dissolution. It exhibits more negative values of E_{corr} and as a result requires lower energy in electrocoagulation. The solubility of alloying elements, such as zinc, magnesium and indium, is low in aluminium at room temperature and in addition to the solid solution formed on alloying, precipitates of indium, zinc and magnesium may exist. Although the treatment process and temperature will influence the solubility of these alloying elements, the solubility of magnesium in aluminium is about 1% at room temperature and magnesium precipitation begins at the grain boundaries as Al_3Mg_2 or Al_8Mg_5 [29,30]. These intermetallics provide sites for localised attack [30]. Although, this attack is less evident for Al–Mg alloys containing less than 3% magnesium, it is likely that the peculiar form of pitting which was observed in NaCl solutions, Fig. 3(b), is due to preferential attack at these intermetallic compounds. For the Al–Zn–In alloy, a large number of small pits are distributed across the surface suggesting that it is the indium and zinc in solid solution that has the greatest impact on the dissolution of the alloy.

5. Conclusions

Two alloys, Al–Mg and Al–Zn–In, were used as anodes in an electrocoagulation cell to remove phosphates, Zn^{2+} and Orange II. Good removal efficiencies were observed for both alloys, but the presence of the indium and zinc alloying elements enhanced the performance of the Al–Zn–In alloy. This was attributed to the instability of the passive film that formed on the Al–Zn–In alloy that enhanced dissolution and the production of Al^{3+}. These results highlight the advantage of using an aluminium alloy activated with zinc and indium, that is less susceptible to localised pitting attack, in electrocoagulation.

Acknowledgements

The authors would like to acknowledge funding from the Irish Research Council, EMBARK initiative.

References

[1] G.H. Chen, Electrochemical technologies in wastewater treatment, Sep. Purif. Technol. 38 (2004) 11–41.
[2] M. Kobya, O.T. Can, M. Bayramoglu, Treatment of textile wastewaters by electrocoagulation using iron and aluminum electrodes, J. Hazard. Mater. 100 (2003) 163–178.
[3] S. Garcia–Segura, M.M.S.G. Eiband, J. Vieira de Melo, C.A. Martinez–Huitle, Electrocoagulation and advance electrocoagulation processes: a general review about the fundamentals, emerging applications and its association with other technologies, J. Electroanal. Chem. 801 (2017) 267–299.
[4] M. Elazzouzi, Kh. Haboubi, M.S. Elyoubi, Electrocoagulation flocculation as a low-cost process for pollutants removal from urban wastewater, Chem. Eng. Res. Des. 117 (2017) 614–626.
[5] P.K. Holt, G.W. Barton, C.A. Mitchell, The future for electrocoagulation as a localized water treatment technology, Chemosphere 59 (2005) 355–367.
[6] G. Sharma, J. Choi, H.K. Shon, S. Phuntsho, Solar-powered electrocoagulation system for water and wastewater treatment, Desalin. Water Treat. 32 (2011) 381–388.
[7] I. Ali, T.A. Khan, M. Asim, Removal of arsenate from groundwater by electrocoagulation method, Environ. Sci. Pollution Res. 19 (2012) 1668–1676.
[8] F.Y. AlJaberi, W.T. Mohammed, The most practical treatment methods for wastewaters: a systematic review, Mesop. Environ. J. 5 (1) (2018) 1–18.
[9] N. Balasubramanian, T. Kojima, C. Srinivasakannan, Arsenic removal through electrocoagulation: kinetic and statistical modeling, Chem. Eng. J. 155 (2009) 76–82.
[10] F. Yasir AlJaberi, Studies of autocatalytic electrocoagulation reactor for lead removal from simulated wastewater, J. Environ. Chem. Eng. 6 (2018) 6069–6078.
[11] E. Lacasa, P. Canizares, C. Saez, F.J. Fernandez, M.A. Rodrigo, Electro–chemical phosphates removal using iron and aluminium alloys, Chem. Eng. J. 172 (2011) 137–143.
[12] K.MansouriK. Ibrik, N. Bensalah, A. Abdel–Wahab, Anodic dissolution of pure aluminium during electrocoagulation process: influence of supporting electrolyte, initial pH, and curent density, Ind. Eng. Chem. Res. 50 (2011) 13362–13372.
[13] I. Kabdaşlı, I. Arslan–Alaton, T. Ölmez–Hancı, O. Tünay, Electrocoagulation applications for industrial wastewaters: a critical review, J. Environ. Technol. Rev. 1 (2012) 2–45.
[14] L.C. Abodi, J.A. DeRose, S. Van Damme, A. Demeter, T. Suter, J. Deconinck, Modeling localized aluminum alloy corrosion in chloride solutions under non–equilibrium conditions: steps toward understanding pitting initiation, Electrochim. Acta 63 (2012) 169–178.
[15] K.–H. Na, S.–l. Pyun, Effect of sulphate and molybdate ions on pitting corrosion of aluminium by using electrochemical noise analysis, J. Electroanal. Chem. 596 (2006) 7–12.
[16] K.–H. Na, S.I. Pyun, Effects of sulphate, nitrate and phosphate on pit initiation of pure aluminium in HCl–based solution, Corros. Sci. 49 (2007) 2663–2675.
[17] M. Mechelhoff, G.H. Kelsall, N.J.D. Graham, Electrochemical behaviour of aluminum in electrocoagulation processes, Chem. Eng. Sci. 95 (2013) 301–312.
[18] C.B. Breslin, L.P. Friery, The Synergistic Interaction Between Indium and Zinc in the Activation of Aluminium, Corros. Sci. 36 (1994) 231–240.
[19] C.B. Breslin, L.P. Friery, W.M. Carroll, The Electrochemical Behaviour of Al–Zn–In and Al–Zn–Hg Alloys in Aqueous Halide Solutions, Corros. Sci. 36 (1994) 85–97.
[20] OECD, Test No. 303: Simulation Test – Aerobic Sewage Treatment – a: Activated Sludge Units; B: Biofilms, in: OECD Guidelines for the Testing of Chemicals, Adopted 22 January (2011).
[21] G. Gonzales, E. Touraud, S. Spinelli, O. Thomas, Organic constituents, in: O. Thomas, C. Burgess (Eds.), UV–Visible Spectrophotometry of Water and Wastewater, Elsevier, 2007.
[22] O. Guseva, P. Schmutz, T. Suter, O. von Trzebiatowski, Modelling of anodic dissolution of pure aluminium in sodium chloride, Electrochim. Acta 54 (2009) 4514–4524.
[23] G. Eriksson, An algorithm for the computation of aqueous multicomponent, multiphase equilibriums, Anal. Chim. Acta 112 (1979) 375–383.
[24] S. Irdemez, Y.S. Yildiz, V. Tosunoglu, Optimization of phosphate removal from wastewater by electrocoagulation with aluminum plate electrodes, Sep. Purif. Technol. 52 (2006) 394–401.
[25] N. Bektas, H. Akbulut, H. Inan, A. Dimoglio, Removal of phosphate from aqueous solutions by electro–coagulation, J. Hazard. Mater. 106 (2004) 101–105.
[26] X.Y. Zheng, H.N. Kong, D.Y. Wu, C. Wang, Y. Li, H.R. Ye, Phosphate removal from source separated urine by electrocoagulation using iron plate electrodes, Water Sci. Technol. 60 (2009) 2929–2938.
[27] X. Chen, P. Ren, T. Li, J.P. Trembly, X. Liu, Zinc removal from model wastewater by electrocoagulation: processing, kinetics and mechanism, Chem. Eng. J. 349 (2018) 358–367.
[28] I. Heidmann, W. Calmano, Removal of Zn(II), Cu(II), Ni(II), Ag(I) and Cr(VI) present in aueous solutions by aluminium electrocoagulation, J. Hazard. Mater. 152 (2008) 934–941.
[29] J.R. Davis, Corrosion of Aluminum and Aluminum Alloys, ASM International, 1999.
[30] Uhlig's Corrosion Handbook, 2nd ed., John Wiley & Sons, Inc, 2000.